


Expanding the Horizons of Hierarchical Zeolites: Beyond Laboratory Curiosity towards Industrial Realization

Working Paper**Author(s):**

Pérez-Ramírez, Javier; Mitchell, Sharon; Verboekend, Danny; Milina, Maria; Michels, Nina-Luisa; [Krumeich, Frank](#) ; Marti, Nadia; Erdmann, Mandy

Publication date:

2011

Permanent link:

<https://doi.org/10.3929/ethz-a-010792708>

Rights / license:

[In Copyright - Non-Commercial Use Permitted](#)

Expanding the Horizons of Hierarchical Zeolites: Beyond Laboratory Curiosity towards Industrial Realization**

Javier Pérez-Ramírez,* Sharon Mitchell, Danny Verboekend, Maria Milina, Nina-Luisa Michels, Frank Krumeich, Nadia Marti, Mandy Erdmann

In recent years, we have witnessed remarkable progress in the preparation, characterization, and application of hierarchical (mesoporous) zeolites.^[1] This wave of research originated because conventional (purely microporous) zeolites, despite being dressed with a truly unique combination of properties, underperform in many relevant reactions due to diffusion constraints. The introduction of auxiliary mesoporosity in zeolite crystals, which improves micropore accessibility and molecular transport,^[2] enhances their activity, selectivity, and lifetime in a large number of heterogeneously catalyzed reactions.^[3] Besides the benefits in catalysis, mesoporous zeolites exhibit improved performance in adsorption and ion-exchange processes.^[4]

To date, the preparation of mesoporous zeolites has been confined to the laboratory scale, undertaken in gram quantities under precisely controllable conditions. Many of the routes developed are cost prohibitive and currently unthinkable for large-scale production. Furthermore, characterization and catalytic studies have encircled pure zeolite powders. Often, advanced porous materials do not make it to real-life processes due to the difficulties encountered in extrapolating encouraging laboratory results to an industrial context. Therefore, to truly ascertain future perspectives of mesoporous zeolites, it is of urgent precedence to demonstrate 1) their large-scale preparation and 2) the preservation of their enhanced properties upon shaping into a workable form. The former need requires the identification of scalable and economically viable preparation methods, whereas the latter constitutes the formation of a hierarchical material in the broadest dimension, integrating the micro-, meso-, and macroporosity levels in a complex zeolite-binder body. This communication reports the first large-scale preparation

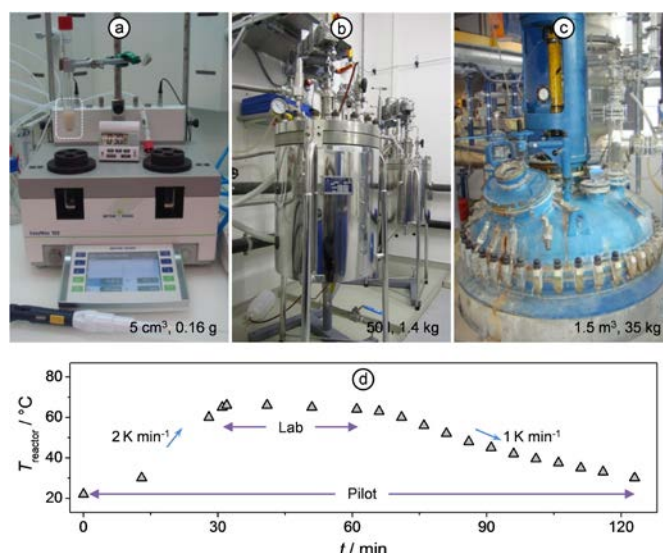


Figure 1. a) Laboratory, b) middle, and c) pilot set-ups used for zeolite desilication. The volumes of alkaline solution and amounts of ZSM-5 treated are given. d) Different temperature profiles during the laboratory- and pilot-scale treatments.

of such hierarchically structured zeolite catalysts.

A primary objective was to reproducibly introduce extensive intracrystalline mesoporosity into ZSM-5. For this purpose, controlled silicon extraction in alkaline medium (desilication)^[5] was performed over a zeolite in laboratory, middle, and pilot scales (Figures 1a-c, respectively, and Table 1). The parent zeolite (P) with Si/Al = 39 possesses pure MFI structure (Figure S11) and the characteristic type I N₂ isotherm (Figure 2). Its morphology is typical of a commercial zeolite, consisting of particles in the range 0.5–4 μm. Each particle (see example in Figure 3a) comprises an aggregate of individual crystals of well-defined cubic shape (Figure 3b). Lab-scale alkaline treatment (0.2 M NaOH, 338 K, 30 min) led to ML, which possessed a 3.5 times greater mesopore surface area (*S*_{meso}) than the parent zeolite. The combined type I and IV behavior observed in the N₂ isotherm is a typical fingerprint of mesoporosity development upon controlled silicon extraction, with pores centered at approximately 10 nm (Figure 2).

Table 1. Zeolite composition and porosity data.

Sample (code)	Si/Al ^[a] [-]	V _{pore} ^[b] [cm ³ g ⁻¹]	V _{micro} ^[c] [cm ³ g ⁻¹]	S _{meso} ^[c] [m ² g ⁻¹]	S _{BET} ^[d] [m ² g ⁻¹]
Parent (P)	39	0.25	0.15	71	431
Parent granule (P-G)	32	0.28	0.12	85	375
Mesoporous lab (ML)	28	0.60	0.11	255	537
Mesoporous mid (MM)	28	0.66	0.12	245	541
Mesoporous pilot (MP)	28	0.56	0.12	256	544
Mesoporous granule (MP-G)	23	0.65	0.11	205	408

[a] Molar ratio in solid, determined by AAS. [b] Volume of N₂ adsorbed at a relative pressure (*p/p*₀) of 0.99. [c] *t*-plot method^[6a]. [d] BET method^[6b].

[*] Prof. J. Pérez-Ramírez, Dr. S. Mitchell, D. Verboekend, M. Milina, N. M. Michels
Institute for Chemical and Bioengineering
Department of Chemistry and Applied Biosciences
ETH Zurich
Wolfgang-Pauli-Strasse 10, HCI E 125, CH-8093 Zurich, Switzerland
Fax: (+41) 44 6331405
E-mail: jpr@chem.ethz.ch

Dr. Frank Krumeich
Laboratory of Inorganic Chemistry
Department of Chemistry and Applied Biosciences
ETH Zurich
Wolfgang-Pauli-Strasse 10, CH-8093 Zurich, Switzerland

Dr. N. Marti, Dr. M. Erdmann
Zeochem AG
Seestrasse 108, CH-8707 Uetikon, Switzerland

[**] Financial support by the Swiss National Science Foundation (Project number 200021-134572) is acknowledged. We thank the Electron Microscopy Centre of the Swiss Federal Institute of Technology (EMEZ).

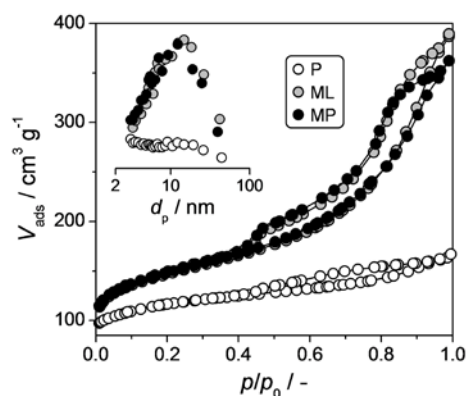


Figure 2. N_2 isotherms of the zeolites. Inset: Barrett-Joyner-Halenda (BJH) adsorption pore size distributions [6c]. d_p = pore diameter.

Practical aspects associated with the large-scale preparation of mesoporous zeolites invoked certain modification of the laboratory-scale treatment procedure. Most notably, the temperature program, was adjusted to conform to restrictions imposed with respect to materials handling and manipulation (Figures 1d). Treatment of 35 kg of parent zeolite in a 1.5 m³ reactor (Figure 1c) produced a hierarchical zeolite (MP) with nearly identical composition and porous properties as ML (Table 1 and Figure 2). Our experience in large-scale zeolite synthesis and modification enables us to confidently state that results from the 1.5 m³ reactor can be reliably extrapolated to the plant scale. Intermediate experiments in a 50 L reactor (Figure 1b) reaffirmed the reproducibility of desilication for mesoporosity generation (MM, Table 1). Monitoring textural changes during alkaline treatment revealed that the principal increase in S_{meso} occurred rapidly during initial reactor heating, reaching a maximum value of about 250 m² g⁻¹. This remained constant throughout further treatment (Figure S12, Supporting Information).

TEM measurements reveal the higher beam transparency of MP (Figure 3c) compared to P (Figure 3a), owing to its increased mesoporosity. However, the size of the crystal aggregates does not change significantly. This aspect is advantageous for the next forming step because a method similar to that for conventional zeolites can be applied to the mesoporous counterpart. Detailed examination of MP by HRTEM shows that the well-defined morphology of the parent (Figure 3b) is mostly retained in the alkaline-treated zeolite (Figure 3d). Although crystallites of the P exhibit uniform contrast, areas of lighter contrast in MP are associated with the presence of intracrystalline mesopores. The homogeneous distribution of mesopores throughout the zeolite crystal aggregate is clearly observable by dark-field scanning transmission electron microscopy (STEM, Figure SI3, Supporting Information). A very narrow crystalline rim, approximately 10 nm in width, remains intact around the edge of the mesoporous zeolite crystallites (Figure 3d). The presence of this rim in the desilicated samples may be related to Al enrichment at the surface of the parent zeolite.^[7] The crystallinity of the alkaline-treated zeolite was confirmed by the observation of lattice fringes, and of sharp diffraction patterns, when analyzed using selected area electron diffraction (SAED, Figure 3e). The long-range order measured by powder XRD was also preserved (Figure SI1, Supporting Information). Additional characterization of P, ML, and MP by IR, ²⁷Al MAS NMR, and NH₃-TPD provided results typical of conventional and alkaline-treated ZSM-5 (Figures SI4-SI6), further stressing the equivalent properties of the mesoporous zeolites prepared in laboratory and pilot scales.

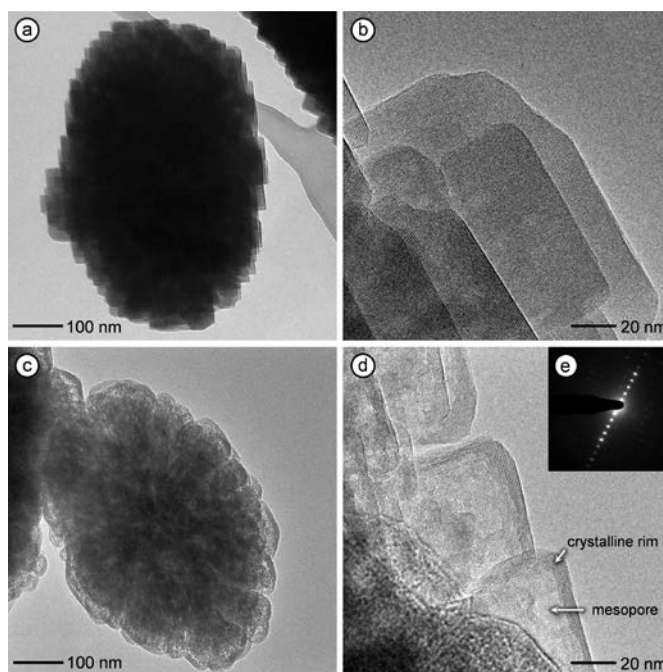


Figure 3. TEM images of the parent zeolite, sample P (a-b) and the pilot alkaline-treated zeolite, sample MP (c-d). The insert (e) shows selected area electron diffraction pattern of crystal rim.

To confirm the improved catalytic properties of the pilot-prepared mesoporous zeolite, three reactions were evaluated: 1) benzene alkylation with benzyl alcohol, 2) benzene alkylation with ethylene, and 3) polyethylene pyrolysis. In all cases, the superior performance of the mesoporous zeolites is attributed to the improved micropore accessibility and molecular transport. The enhanced catalytic performance of MP is immediately apparent for the alkylation of benzene with benzyl alcohol (Figure 4), in which a 50% conversion of benzyl alcohol is achieved after 2 min, reaching 100% after 15 min. For the purely microporous P zeolite, a 50% conversion is only reached after reaction for 25 min. Comparably for the alkylation of benzene with ethylene, the enhancement in catalytic performance of the mesoporous zeolite gave a 4-fold increase in ethylbenzene productivity during benzene alkylation with ethylene (Table SI1, Supporting Information). The higher ethylbenzene selectivity over ML and MP was consistent with the shorter diffusion path lengths in the micropores as a consequence of the introduction of intracrystalline mesoporosity. The formation of polyalkylated products was more prevalent with the purely microporous zeolite. Furthermore, in the pyrolysis of low-density polyethylene, a decrease in the light-off temperature was clearly visible in the thermal analysis (Figure SI7, Supporting Information). The corresponding reduction in T_{50} , the temperature at which 50% LDPE conversion is achieved, was 35 K.

Having found a reliable and cost-effective preparation method, the next step was to consider how the desilicated zeolite could be formed into practical shapes. The mesoporous ZSM-5 zeolite was bound in a pan granulator, using attapulgite (20 wt.%) as a binder, resulting in the isolation of granules of 2-5 mm fractional size (MP-G, Figure 5a). In contrast to our previous work,^[8] we opted to shape a mesoporous zeolite, instead of alkaline treating a bound conventional zeolite. In this way damage to the binder, inter-particle interactions, and consequential modification or loss of structural integrity may be avoided. The binder used, attapulgite, was selected for forming because of its readily identifiable needle-like morphology, which permits facile identification of the component phases by means of microscopic techniques. N_2 adsorption

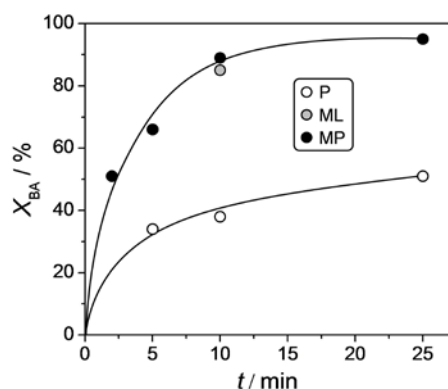


Figure 4. Conversion of benzyl alcohol (BA) over the zeolites in benzene alkylation with benzene alcohol.

confirmed that the mesopore surface area was not blocked by the binder, because the bound hierarchical zeolite possesses a mesoporous surface area of $205 \text{ m}^2 \text{ g}^{-1}$ (Table 1 and Figure SI8, Supporting Information). The small reduction in N_2 uptake arose from the inclusion of the attapulgite binder, which has a lower porosity. No significant morphological alterations are observed in either of the component phases after forming. The binder is clearly visible by SEM and TEM, decorating the surface of the mesoporous ZSM-5 particles (Figures 7b-c). Mercury porosimetry (Figure 5d) provided additional on the porous structure of the granules. In addition to the network of intracrystalline mesopores around 10 nm, a macroporous network centered at 140 nm coexisted (inset of Figure 5d). The latter mostly arose from interparticle spaces between the needle-like binder particles, which were highly dispersed during granulation. As expected, the granule of the parent zeolite (P-G) did not show a contribution in the mesopore range. The mechanical properties of the conventional and mesoporous zeolite granules were equivalent based on crush strength and attrition tests.

In conclusion, we successfully demonstrate the large-scale preparation of hierarchical zeolites. The robustness of the desilication route is clearly established by the identical properties of the mesoporous zeolites prepared on laboratory, middle, and pilot scales, despite necessary adaption of the standard procedure. We presented unequivocal evidence for the enhanced catalytic properties of mesoporous zeolites in different test reactions. Finally, in fundamental work, the formation of hierarchically structured zeolite granules was also reported. This paves the way for future research in the subsequent key steps in the design of mesoporous zeolites for various applications. In subsequent studies, structure-performance relationships of the hierarchical zeolite bodies in catalytic and adsorption processed will be addressed.

Experimental Section

ZSM-5 zeolite with Si/Al ratio = 40 was synthesized hydrothermally at 1 MPa in an industrial 1.5 m^3 autoclave. The reactor was charged stepwise with water, colloidal silica, sodium aluminate, tetrapropyl ammonium bromide, and sodium hydroxide. The final gel, containing 82.23 mol SiO_2 , 1.00 mol Al_2O_3 , 5.56 mol Na_2O , 2.36 mol TPABr, and 1373.50 mol H_2O , was homogenized and heated to 423 K at 0.83 K min^{-1} . After 24 h, the reactor was cooled, and the zeolite was filtered (Fundabac, Dr. M), washed with distilled water, and dried at 333 K for 12 h in a Nabertherm furnace using air convection. Template removal was achieved in the same furnace by calcination in flowing dry air at 753 K for 3 h. The amount of zeolite product was 170 kg. Desilication of calcined ZSM-5 in aqueous 0.2 M NaOH was carried out in batch reactors of 5 cm^3 (Easymax 102, Mettler Toledo),

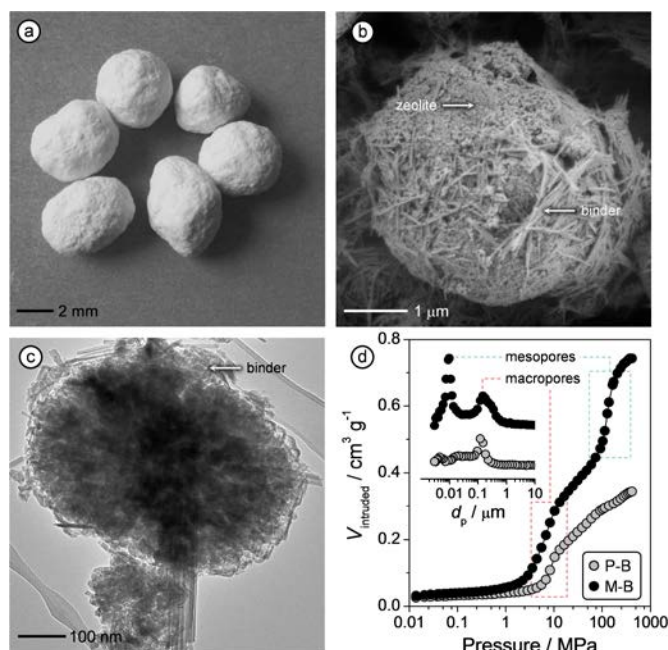


Figure 5. Mesoporous zeolite granules, sample MP-G (a). The SEM and TEM image of MP-G (b and c, respectively) show that the distribution of binder in the agglomerates of mesoporous ZSM-5 crystals. (d) Mercury intrusion curves of the granules and derived pore size distributions (inset).

50 L (Juchheim), and 1.5 m^3 (home-made) (Figure 1). The liquid:solid ratio was fixed at 30 cm^3 of alkaline solution per gram of zeolite. In lab-scale the zeolite was treated isothermally at 338 K for 30 min using magnetic stirring, followed by quenching in ice-water.^[5b] Upscale treatments were conducted under mechanical stirring and incorporated ramped heating and cooling (Figures 1d and SI2). The alkaline-treated (mesoporous) zeolites were filtered, washed, converted to the ammonium form (0.1 M, NH_4NO_3 6 h), and calcined at 823 K for 5 h at 5 K min^{-1} . The hierarchical zeolite powder coming from the pilot reactor was shaped into mm-sized granules using a pan granulator (Eirich) and attapulgite in a zeolite:attapulgite (mass) ratio = 80:20. Si and Al concentrations in the solids were determined by atomic absorption spectroscopy (AAS) using a Varian SpectraAA 220 FS instrument. Nitrogen adsorption was measured at 77 K with a Quantachrome Quadrasorb-SI gas adsorption analyzer. Prior to the measurement, the samples were evacuated at 573 K for 12 h. Mercury-intrusion porosimetry experiments were performed using a Micromeritics Autopore II 9215, which operated in the pressure range from vacuum to 400 MPa. Degassing was undertaken in situ. Transmission electron microscopy (TEM) was carried out in a Phillips CM12 instrument operated at 100 kV. High-resolution HRTEM, selected area electron diffraction (SAED), and energy dispersive X-ray (EDX) measurements were performed with a FEI Tecnai F30 microscope operated at 300 kV. SEM images of a resin-embedded granule were obtained by using a Zeiss Gemini 1530FEG microscope operated at 1 kV. The alkylation of benzene with benzyl alcohol was conducted in an Endeavor Catalyst Screening System (Argonaut Technologies). Reaction conditions were $P = 0.5 \text{ MPa}$, $T = 433 \text{ K}$, benzene:benzyl alcohol (molar) ratio = 80, and 40 wt.% zeolite with respect to benzyl alcohol. Liquid products were analyzed by gas chromatograph (HP 6890) coupled to a mass selective detector (HP 5973). Additional characterization and catalytic studies are described in the Supporting Information.

Received: ((will be filled in by the editorial staff))

Published online on ((will be filled in by the editorial staff))

Keywords: zeolites • heterogeneous catalysis • hierarchical materials • desilication • scale up

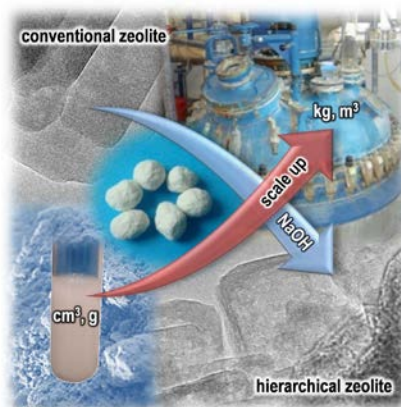
-
- [1] a) S. van Donk, A. H. Janssen, J. H. Bitter, K. P. de Jong, *Catal. Rev. -Sci. Eng.* **2003**, *45*, 297; b) M. Hartmann, *Angew. Chem.* **2004**, *116*, 6004; c) L. Tosheva, V. P. Valtchev, *Chem. Mater.* **2005**, *17*, 2494; d) Y. Tao, H. Kanoh, L. Abrams, K. Kaneko, *Chem. Rev.* **2006**, *106*, 896; e) J. Čejka, S. Mintova, *Catal. Rev. -Sci. Eng.* **2007**, *49*, 457; f) J. Pérez-Ramírez, C. H. Christensen, K. Egeblad, C. H. Christensen, J. C. Groen, *Chem. Soc. Rev.* **2008**, *37*, 2530; g) K. Egeblad, C. H. Christensen, M. Yu. Kustova, C. H. Christensen, *Chem. Mater.* **2008**, *20*, 946; f) W. Schmidt, W. *ChemCatChem* **2009**, *1*, 53; h) R. Chal, C. Gérardin, M. Bulut, S. van Donk, *ChemCatChem* **2011**, *3*, 67.
- [2] a) J. C. Groen, W. Zhu, S. Brouwer, S. J. Huynink, F. Kapteijn, J. A. Moulijn, J. Pérez-Ramírez, *J. Am. Chem. Soc.* **2007**, *129*, 355; b) L. Zhao, B. Shen, J. Gao, Ch. Xu, *J. Catal.* **2008**, *258*, 228; c) K. Cho, H. S. Cho, L. C. de Menorval, R. Ryoo, *Chem. Mater.* **2009**, *21*, 5664; d) F. Thibault-Starzyk, I. Stan, S. Abelló, A. Bonilla, K. Thomas, C. Fernandez, J.-P. Gilson, J. Perez-Ramirez, *J. Catal.* **2009**, *264*, 11.
- [3] a) C. H. Christensen, K. Johannsen, I. Schmidt, C. H. Christensen, *J. Am. Chem. Soc.* **2003**, *125*, 13370; b) M. Choi, H. S. Cho, R. Srivastava, C. Venkatesan, D.-H. Choi, R. Ryoo, *Nat. Mater.* **2006**, *5*, 718; c) J. Pérez-Ramírez, D. Verboekend, A. Bonilla, S. Abelló, *Adv. Funct. Mater.* **2009**, *19*, 3972; d) K. P. de Jong, J. Zečević, H. Friedrich, P. E. de Jongh, M. Bulut, S. van Donk, R. Kenmogne, A. Finiels, V. Hulea, F. Fajula, *Angew. Chem. Int. Ed.* **2010**, *49*, 10074; e) M. S. Holm, E. Taarning, K. Egeblad, C. H. Christensen, *Catal. Today* **2011**, doi:10.1016/j.cattod.2011.01.007.
- [4] a) R. Le Van Mao, S. Xiao, A. Ramsaran, J. Yao, *J. Mater. Chem.* **1994**, *4*, 605; b) I. Melián-Cabrera, S. Espinosa, J. C. Groen, B. v/d Linden, F. Kapteijn, J. A. Moulijn, *J. Catal.* **2006**, *238*, 250; c) J. Yang, Y. Zhou, W. G. Lin, Y. J. Wu, N. Lin, J. Wang, J. H. Zhu, *J. Phys. Chem. C* **2010**, *114*, 9588.
- [5] a) M. Ogura, S. -Y. Shinomiya, J. Tateno, Y. Nara, M. Nomura, E. Kikuchi, M. Matsukata, *Appl. Catal. A* **2001**, *219*, 33; b) J. C. Groen, L. A. A. Peffer, J. A. Moulijn, J. Pérez-Ramírez, *Chem. Eur. J.* **2005**, *11*, 4983; c) J. C. Groen, J. A. Moulijn, J. Pérez-Ramírez, *J. Mater. Chem.* **2006**, *16*, 2121.
- [6] a) S. Brunauer, P. H. Emmett, E. Teller, *J. Am. Chem. Soc.* **1938**, *60*, 309; b) B. C. Lippens, J. H. de Boer, *J. Catal.* **1965**, *4*, 319; c) E. P. Barrett, L. G. Joyner, P. P. Halenda, *J. Am. Chem. Soc.* **1951**, *73*, 373.
- [7] a) J. C. Groen, T. Bach, U. Ziese, A. M. Paulaime-van Donk, K. P. de Jong, J. A. Moulijn, J. Pérez-Ramírez, *J. Am. Chem. Soc.* **2005**, *127*, 10792. b) N. Danilina, F. Krumeich, S. A. Castelanelli, J. A. van Bokhoven, *J. Phys. Chem. C* **2010**, *114*, 6640.
- [8] J. C. Groen, J. A. Moulijn, J. Pérez-Ramírez, *Ind. Eng. Chem. Res.* **2007**, *46*, 4193.

Entry for the Table of Contents

Zeolites

Javier Pérez-Ramírez,* Sharon Mitchell, Danny Verboekend, Maria Milina, Nina-Luisa Michels, Frank Krumeich, Nadia Marti, Mandy Erdmann

Expanding the Horizons of Hierarchical Zeolites: Beyond Laboratory Curiosity towards Industrial Realization



Scale up for the win! Hierarchically structured zeolites are prepared on a large scale by desilication followed by forming into mm-sized bodies. Extrapolation of the superior catalytic properties is proven by the remarkable similarity between pilot and laboratory scale results. The binder and the shaping process do not alter the enhanced porous properties of the mesoporous zeolite. These results unlock the door towards the study of further key steps in the design of mesoporous zeolite catalysts for large scale applications.

Supporting Information

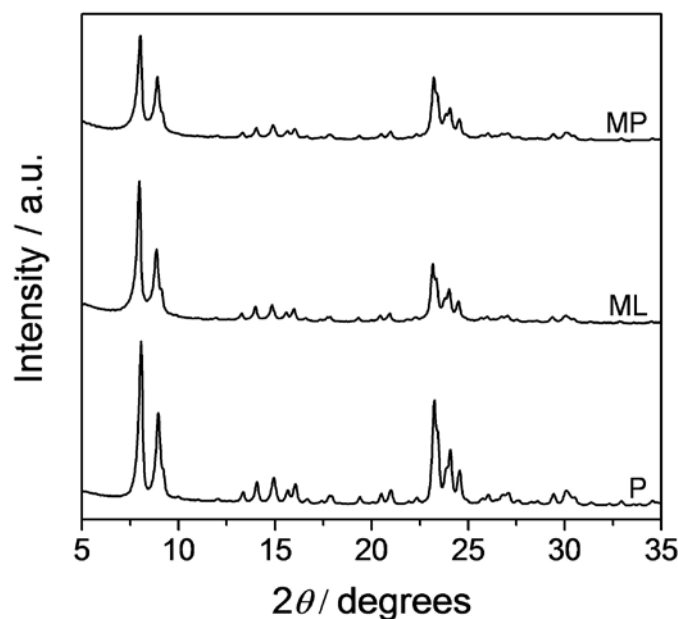


Figure SI1. Powder X-ray diffraction (XRD) patterns of the zeolites. X-ray diffraction was measured in a PANalytical X'Pert PRO-MPD diffractometer equipped with an X'Celerator linear detection system. Data were recorded in the range 5-50° 2θ, with an angular step size of 0.05° and a counting time of 8 s per step. The long-range crystallinity in the parent zeolite is preserved upon mesoporosity introduction by alkaline treatment.

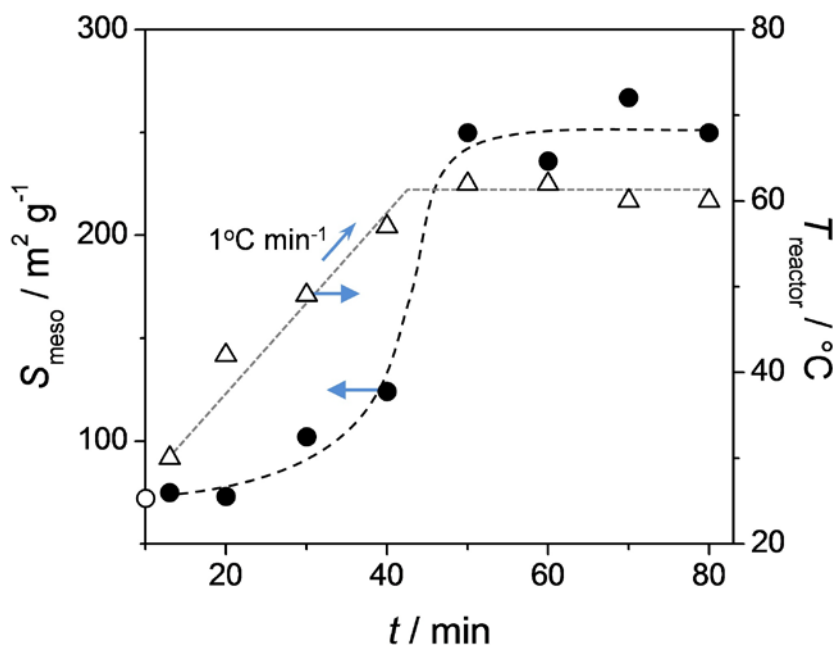


Figure SI2. Temperature profile (open triangles) and corresponding variation in zeolite mesopore surface area (S_{meso} , solid circles) during alkaline treatment in a 50 L reactor (mid-scale). Slurry probes (50 cm³) were taken at regular, quenched in ice, and the zeolite was isolated by filtration, washed, and dried, prior to characterization by N₂ adsorption. The open circle on the left y-axis corresponds to the S_{meso} of the parent ZSM-5.

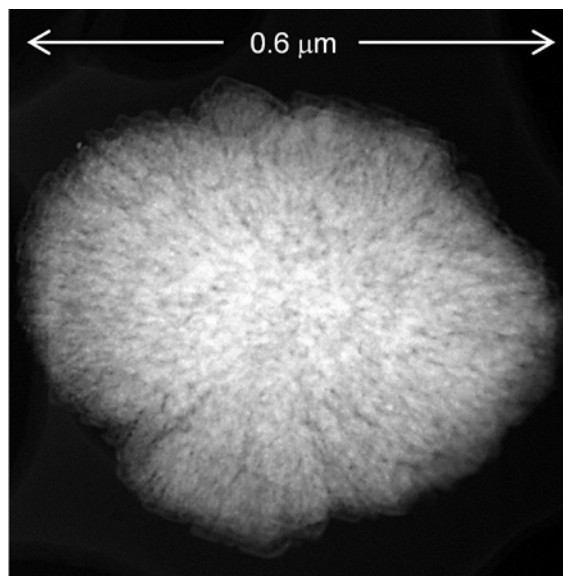


Figure SI3. Dark-field scanning transmission electron microscopy (STEM) image of the mesoporous zeolite prepared in the pilot reactor (MP). STEM was undertaken using an aberration-corrected HD-2700CS microscope (Hitachi) operated at 200 kV. The uniform mesoporosity distribution along the crystal aggregate can be clearly seen.

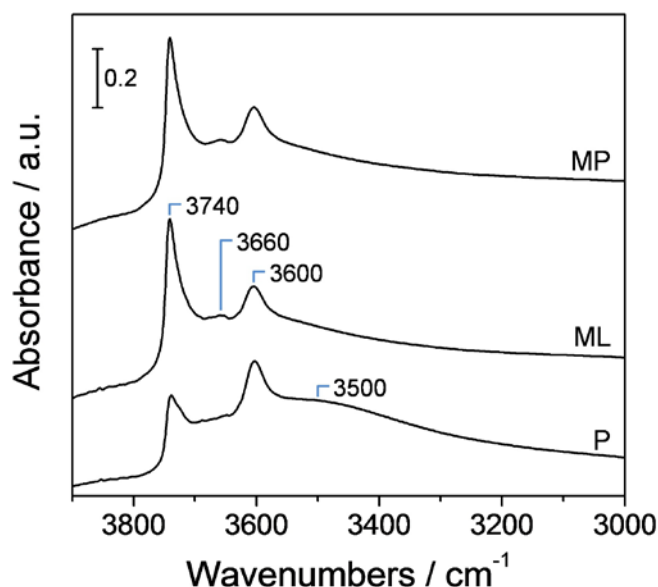


Figure SI4. Fourier transform infrared spectra (FTIR) of the zeolites in the hydroxyl stretching region. Analyses were performed in nitrogen atmosphere at 473 K using a Thermo Nicolet 5700 spectrometer using a SpectraTech Collector II diffuse reflectance accessory and equipped with a high-temperature cell. Prior to the measurement, the sample was dried at 573 K in N₂ flow (100 cm³ min⁻¹) for 60 min. Spectra were recorded in the range of 650-4000 cm⁻¹ with a nominal resolution of 4 cm⁻¹ and co-addition of 100 scans. Alkaline treatment of P leads to an increased presence of isolated external silanol groups (3740 cm⁻¹), and a reduced amount of interacting silanol groups associated with internal defects (3500 cm⁻¹), while little variation in strong Brønsted acid sites (3600 cm⁻¹), or in the band which has recently been ascribed to partially hydrolyzed framework Al (3660 cm⁻¹), is observed. No evidence of extra-framework Al (3780 cm⁻¹) is visible. Band assignments were taken from Bleken *et al. Phys. Chem. Chem. Phys.* **2011**, *13*, 2539.

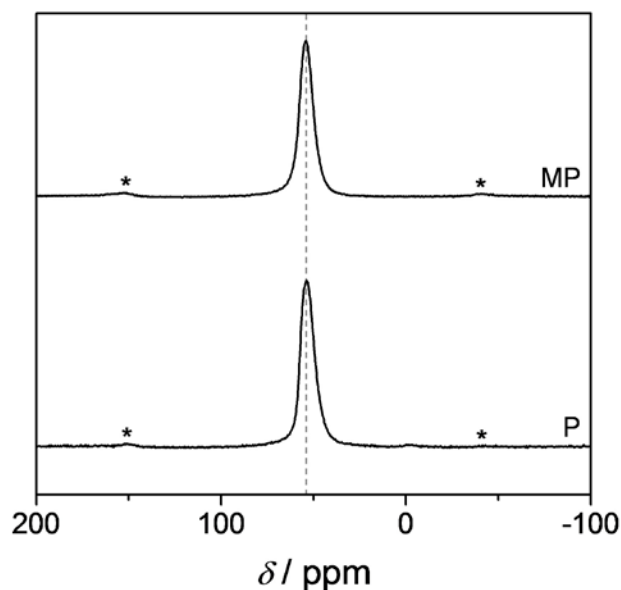


Figure SI5. ^{27}Al magic angle nuclear magnetic resonance (MAS NMR) spectra of the P and MP zeolites. ^{27}Al MAS NMR spectroscopy was performed at a spinning speed of 10 kHz on a Bruker Avance 400 NMR spectrometer equipped with a 4 mm probe head and 4 mm ZrO_2 rotors at 104.3 MHz. ^{27}Al spectra were recorded using 2048 accumulations, 90° pulses with a pulse length of 1 μs , a recycle delay of 1 s, and $(\text{NH}_4)\text{Al}(\text{SO}_4)_2 \cdot 12\text{H}_2\text{O}$ as the reference. Asterisks indicate positions of spinning side bands. The single dominant peak at 55 ppm is characteristic of tetrahedral Al in lattice positions of the zeolite. No peak at 0 ppm, typical of octahedral Al in extra-framework positions, was identified.

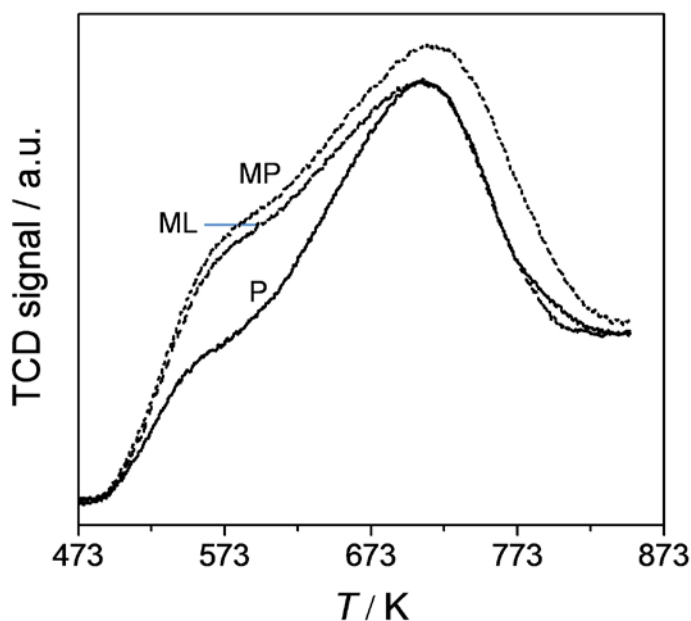


Figure SI6. Temperature-programmed desorption of ammonia (NH_3 -TPD) of the zeolites. Analyses were carried out in a Thermo TPDRO 1100 unit equipped with a thermal conductivity detector. The sample (0.100 g) was pre-treated at 823 K in He ($20 \text{ cm}^3 \text{ min}^{-1}$) for 2 h. Afterwards, NH_3 (10% in He, $20 \text{ cm}^3 \text{ min}^{-1}$) was adsorbed at 473 K for 30 min followed by purging with He at the same temperature for 1 h. This procedure was repeated three times. Desorption of NH_3 in He flow ($20 \text{ cm}^3 \text{ min}^{-1}$) was monitored in the range of 473–1173 K using a ramp rate of 10 K min^{-1} . Alkaline treatment leads to an increase in intensity of the low-temperature desorption peak (shoulder at 600 K), which is attributed to the increased presence of Lewis acid sites. No significant variation is observed in the high-temperature desorption peak, primarily associated with strong Brønsted acid sites.

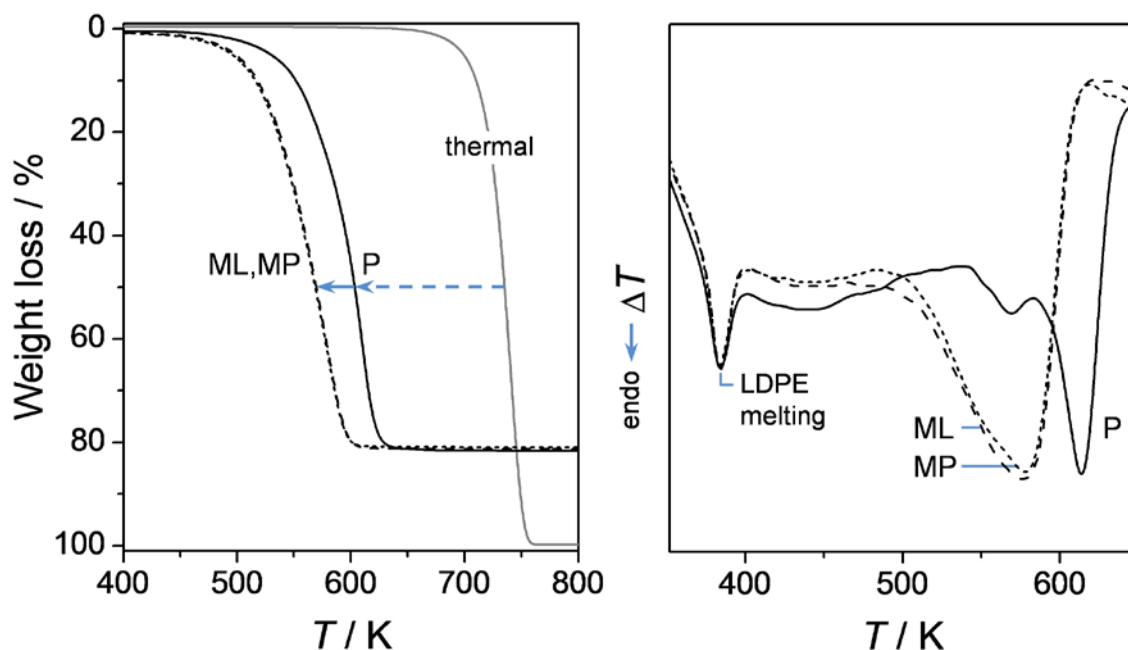


Figure SI7. Weight loss (a) and thermal analysis (b) during LDPE pyrolysis over the zeolites. Low-density polyethylene (LDPE, Alfa Aesar) pyrolysis was carried out in a thermogravimetric analyzer (Mettler Toledo TGA/DSC 1). The polymer and the zeolite, both in powder form, were intimately mixed in a mass ratio 80:20. Pyrolysis was performed in N_2 atmosphere ($70 \text{ cm}^3 \text{ min}^{-1}$) ramping the temperature from 303 to 973 K at 5 K min^{-1} . A lower pyrolysis temperature is obtained over the mesoporous zeolites due to the improved accessibility with respect to the purely microporous counterpart.

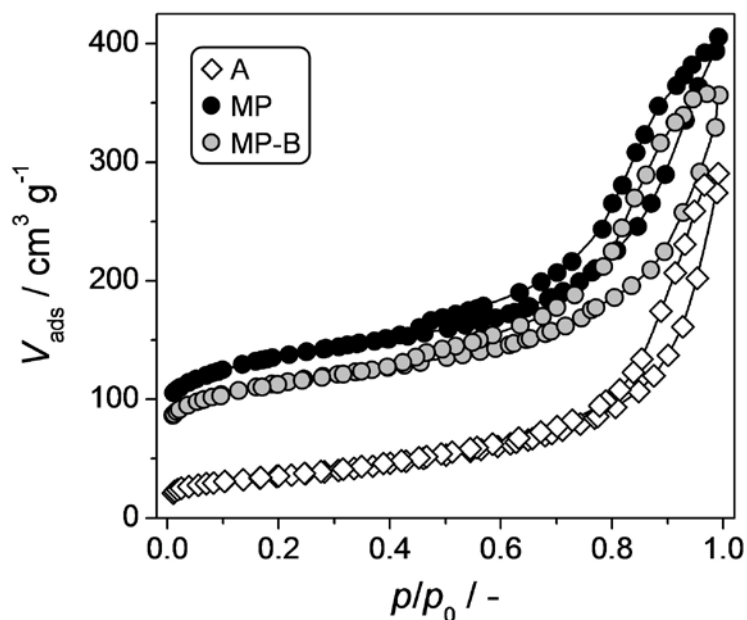


Figure SI8. Nitrogen isotherms of the hierarchical zeolite beads (MP-G), the binder-free mesoporous zeolite powder (MP), and the attapulgite binder powder (A). All the samples were measured in the calcined form. The enhanced porous properties of the mesoporous zeolite obtained by alkaline treatment is affected neither by the presence of the binder nor by the shaping process.

Table SI1. Ethylbenzene (EB) productivity and selectivity of the zeolites in the liquid-phase benzene alkylation with ethylene.

Sample (code)	$P(\text{EB})$ (mmol g _{cat} ⁻¹)	$S(\text{EB})$ (%)
Parent (P)	2	90
Mesoporous lab (ML)	8	98
Mesoporous pilot (MP)	8	98

The liquid-phase alkylation of benzene with ethylene over the zeolites was studied in a 500 cm³ commercial titanium batch autoclave (Premex). First, 200 cm³ of benzene were introduced in the reactor with approximately 100 mg of powdered catalyst that was previously pretreated at 573 K in He for 12 h to remove moisture. After purging with N₂, the reactor was heated to 438 K under mechanical stirring (1000 rpm). Subsequently, ethylene was introduced in the reactor until the molar benzene:ethylene ratio was 4:1 and a total pressure of 23 bar was obtained. During the reaction, liquid aliquots (0.2 cm³) were extracted from the reactor, which were analyzed with a GC (Agilent 6890N) equipped with a CPSil-8B column and an FID detector. Reported data are after a reaction time of 400 min.